Wear and Friction Behavior of Gr/Sn Solid Lubricated Dual Reinforced AMCs

Varun Singhal
Thapar Institute of Engineering and Technology
Om Prakash Pandey (oppandeytu@gmail.com)
Thapar Institute of Engineering & Technology https://orcid.org/0000-0002-6826-995X

Research Article

Keywords: Solid lubricants, Wear and friction, Density, Hardness, LM30 alloy, Sillimanite, Ilmenite

Posted Date: June 21st, 2021

DOI: https://doi.org/10.21203/rs.3.rs-607348/v1

Abstract

The current work has been undertaken to see the effect of Gr/Sn as a solid lubricant for the development of hybrid aluminum metal matrix composite (HAMCs). HAMCs were fabricated by reinforcing 10 wt. % (sillimanite + ilmenite) minerals with or without 1 wt. % Sn/Gr/both solid via stir casting technique. Optical microscopy revealed a homogenous distribution of reinforced particles with the refinement of silicon. Vicker hardness of the HAMCs showed a good interfacial bonding of particles with the matrix. The wear rate and coefficient of friction of the HAMCs are reduced with a maximum of composite with tin and graphite as lubrication agents. The composite contained tin and graphite wear rate as lubrication agents were in tune with the cast-iron brake drum used in the automobile industries. Abrasive wear was dominant at low loads and adhesive wear at high load, as confirmed from SEM analysis.

1. Introduction

In the past few decades, many scientists are searching for a substitute for ferrous metals to increase fuel efficiency for different automobile parts. Aluminum alloy can be considered as the perfect substitute for ferrous material if its strength and hardness are improved. Al-alloys having relatively lower density made revolutionary changes in many sectors of automobile, aeronautical and marine industries for developing lightweight spare parts [1]. Also, Al has specific characteristics like ductility, recyclability, strength to weight ratio [2]. Apart from these properties, its applicability is being compromised in terms of its low hardness, which has been modified by incorporating different ingredients and forming a composite. This exhibits the enhanced properties based on the degree of interfacial bonding of the ingredients mixed homogenously.

Al-Si alloy containing nearly 13 wt. % is the most practiced alloy due to its good castability, low density, and high corrosion resistance [2], [3]. Aluminum matrix composites (AMCs) exhibit a wide range of applications [4]–[6]. Most of the research groups have investigated the properties of AMCs by incorporating (i) synthetic and (ii) natural reinforcement. Synthetic ceramic compounds such as SiO_2 [7], ZrO_2 [8], SiC [9], B_4C [10], Al_2O_3 [11], etc., as reinforcement have shown an excellent wear resistance of Al-alloy matrix composites [12]–[14]. At the same time, natural minerals like rutile [15], garnet [16], zircon [17] etc. can reduce the human efforts by lowering the cost of manufacturing to achieve similar or even better tribological properties along with high corrosion resistance [18]–[22]. Therefore, most research groups use natural minerals to enhance the hardness, wear, and corrosion resistance of Al or its alloys [23]. Sillimanite reinforced in an aluminum matrix such as LM6 [24], LM30 [20] enhances tribological properties. However, these authors have studied the effect of particle size on wear rate on LM6 and LM30 alloy. Moreover, sillimanite has high mechanical (hardness, modulus) and thermal properties. Also, sillimanite is an ore of aluminum. It will improve the wettability between the aluminum matrix and sillimanite. At the same time, ilmenite also has high mechanical properties. Considering these aspects, reinforcement of more than one mineral in the AMCs will be a more effective and cheapest route to enhance AMCs properties. Such hybrid composites (HAMCs) have not been studied extensively.

Gupta et al. [25] concluded that the addition of dual reinforcement (sillimanite + rutile) provided enhancement in wear resistance compared to the composites reinforced with only sillimanite or rutile. Kaushik and Rao [26] observed the formation of intermetallic phase during heat treatment (T6) which helped to reduce wear rate by 27% of dual reinforced (Al-SiC-Gr) composite sample and single reinforced (Al-SiC) composite sample, i.e., 22.9% as compared to Al-6082 alloy.

Moreover, to reduce the seizure wear and friction in pistons and cylinder, solid lubricants like graphite (Gr), tin (Sn), lead (Pb) and $MoS_{2,}$ etc. are added during the manufacturing of composite, which can also provide inherent reduced wear loss [17–19]. Some of the research groups have also studied the effect of solid lubricant in AMCs on their wear behavior. Tyagi [29] and Das et al. [30] suggested the enhancement in interfacial interaction between matrix and individual reinforcements (TiC and graphite, respectively), resulting the enhanced adhesive and seizure wear resistance, respectively. Moreover, tin (Sn) can also be used as a lubricating agent due to its low melting point, which helps fill the surface pores during sliding over the counter surface [2].

The present work is based on the development of HAMCs with both sillimanite (Al_2SiO_5) and ilmenite ($FeTiO_3$) minerals incorporated in LM30 alloy through the stir-casting route which have not been studied so far. Further, a small amount (1 wt. %) of solid lubricants (Gr and Sn) were also incorporated in the prepared composite to study their impact on the wear behavior of hybrid composites. Moreover, from an application point of view, the wear properties of the best HAMCs is also compared with the brake drum material used in the automobile sector.

2. Materials And Method

2.1 Materials

In order to prepare HAMCs, Al-alloy LM30 was obtained from Emmes Metal Pvt. Ltd., Mumbai (India). Natural minerals sillimanite (Al_2SiO_5) and ilmenite ($FeTiO_3$) were procured from Indian Rare Earths Limited, Mumbai (India). The chemical composition of Al-Si alloy and respective reinforcement are enlisted in Table 1.

Sn and Gr were procured from Loba Chemie and was added to melt to reduce friction and wear between two relative sliding surfaces.

Table1: Detail of chemical composition of procured Al-Si alloy (LM30) and reinforcement.

Elements	Concentration (wt. %)	Elements	Concentration (wt. %)	Elements	Concentration (wt. %)
LM30 alloy					
Si	17.7400	**Mg**	0.5200	**Ti**	0.0820
Cu	4.1000	**Zn**	0.2600	**Ca**	0.0180
Fe	0.5300	**Cr**	0.0034	**Pb**	0.0830
Mn	0.1600	**Ni**	0.0023	**Sn**	0.0310
Sr	0.0006	**Al**	Balance		
Sillimanite (wt. %)					
Al_2O_3	58.60	**ZrO_3**	2.20	**Fe_2O_3**	0.40
SiO_3	38.54	**TiO_2**	0.26		
Ilmenite (wt. %)					
TiO_2	55.3	**Al_2O_3**	0.8	**Cr_2O_5**	0.1
FeO	20.5	**SiO_2**	1.6	**MgO**	1.0
Fe_2O_3	19.9	**V_2O_5**	0.2		
Cast iron					
Si	1.66	**Cr**	0.11	**S**	0.12
Fe	93.77	**C**	3.52		
Mg	0.72	**P**	0.10		

2.2 Method

HAMCs samples were produced by stir casting techniques using a graphite stirrer, as shown in Figure 1 [31]. Al-Si alloy (LM30) was melted in a graphite crucible at 750˚C in an electric resistance furnace. In the first step, the molten alloy was stirred at 620 rpm for 4 min. After that, preheated micro-size minerals (1-120 µm) (5 wt. % sillimanite + 5 wt. % ilmenite) were added to the molten alloy after reducing the stirring speed at 265 rpm. These particles were added slowly while stirring. The stirring was continued for 11 min at 620 rpm speed to get uniform distribution of particles in the Al-matrix. Finally, the molten mass was transformed in a 12×12×4 cm^3 rectangular permanent cast-iron mold and left to solidify at room temperature. Another set of composites was also developed with the exact content of minerals but with solid lubricating agents Gr/Sn/both in the molten mass. Table 2 presents the designation of different HAMCs fabricated in the present study.

Table 2: Details of the formulated sample.

Sample ID	Matrix (wt. %)	Amount of different reinforcements (wt. %)			
	LM30	sillimanite	Ilmenite	Sn	Gr
B1	100	-	-	-	-
H1	100	5	5	-	-
HT	100	5	5	1.0	-
HG	100	5	5	-	1.0
HTG	100	5	5	0.5	0.5

2.3 Optical microscopy examination

Further, samples were polished for optical microscopy examination by following the ASTM standard E3-11 (2011). Optical microscope (Eclipse-MA100, Nikon instrument, Tokoyo (Japan) was used to examine the distribution of particles.

2.4 Density and hardness

The Archimedes principle is used to calculate the experimental density (ρ_{ex}) of all prepared samples. Also, theoretical density (ρ_{th}) was calculated through the rule of mixture (Eq.1).

$$\rho_{th} = \rho_1 v_1 + \rho_2 v_2 + \rho_3 v_3 + \rho_4 v_4 + \rho_2 v_2 \quad (1)$$

The Vickers-hardness was measured on the Vicker scale with 100 Kgf load with diamond indenter using the Mitutoyo Vickers hardness instrument model MVKHO. The micro-hardness was taken at three different places (particle, interface, and matrix) as per the ASTM E-92. In addition, the Rockwell hardness of prepared samples was also measured using the Rockwell hardness tester (model no. TRSND, fine manufacturing Industries (India)) at 100 kg load on B-scale for 5 sec dwell time and 1/16'ϕ ball indenter. Both hardness results presented are an average of 5 readings at a given composition.

2.5 Wear and Coefficient of friction measurement

For the wear test, a pin-on-disc setup was used in which a cylindrical pin was mounted on a rotating steel disc. The test was conducted as per ASTM G99 05 (2010) norms. All the tests were performed at 8 mm cylindrical diameter specimens. The test was carried out by varying load at 9.81, 29.43, 49.05, and 68.67 N at a constant velocity of 1.6 m/sec on wear and friction monitor (TR-2L), Ducom Instruments, Bangalore (India). A steel disk of EN32 steel (832 HV hardness) was used as a counter body. In this instrument, the LVDT sensor was used to measure the decrement in height (in μm) of the sample, and wear rate was calculated by using Eq. 2. Before the wear test, samples were ground on 1000 μm grit size paper and cleaned with acetone. This test was performed three times to determine the average wear rate. The friction force was continuously measured during the experiment, and the coefficient of friction (COF) was calculated using Eq. 3.

$$W_R = \frac{H_L \times A_C}{D_S} \quad (2)$$

$$\text{Coefficient of friction (COF)} = \frac{\text{Friction force } (F_f)}{\text{Applied load } (A_L)} \quad (3)$$

Notification:

H_L– Height loss (LVDT sensor display on screen).

A_C – Contact area $(= \frac{\pi}{4} d^2)$, d specimen diameter (mm)

W_R – Wear rate (mm^3/m)

D_S – Sliding distance (=1.6 × time) (m).

2.6 SEM analysis

Scanning electron microscope JOEL, JSM-6510LV, Tokoyo (Japan) evaluated the wear mechanism and compared the structural-tribological relationship at different load conditions.

3. Results And Discussion

3.1 Microscopic examination

3.1.1 Base Material

The optical microstructure of the B1 sample is given in Figure 2 at low and higher magnification. It is observed that the B1 sample contains the coarse primary-Si phase along with the eutectic Al-Si mixture. During the solidification, heterogeneous nucleation occurs inside the molten Al-Si mixture. Thus, primary Si was nucleated as a faceted structure in the α-Al phase. This faceted morphology is like a cube, star, and polygon. At a later stage, solidification of the eutectic mixture occurs where the fine size of Si is shown in figure 2a.

3.1.2 Fabricated composites

It has been observed that the addition of natural minerals (sillimanite + ilmenite) exhibited the outstanding homogeneity of reinforced particles (Figure 3a &b). This was due to the effect of mechanical mixing. During rotation, executed a dynamic shear force between molten alloy and reinforcement particles [3]. The exerted shear force hindered the settling of dense ceramics particles inside the molten alloy, as shown in Figure 3a. Also, there are considerable differences in the thermal conductivity between the matrix and reinforced particles [32]. Thus, the reinforced ceramic particles provided the surface for the

nucleation of the Si phase. Because of many particles inside the molten mass, needle-shaped finer silicon nucleates, as shown in Figure 3a. Moreover, the primary silicon size was also got reduced.

Some research groups have observed the enhancement in mechanical properties of Al-Si alloy as an effect of silicon refinement due to its high hardness [33], [34]. Further, it is a well-known fact that the heat treatment cycle of any alloy/composite manifests the morphological features of prepared samples. Therefore, all the samples were prepared under similar conditions. The EDS line profile of the SEM image indicates the presence of Al, Si, Fe, Ti, and O, showing the presence of sillimanite and ilmenite particles (Figure 3c & d).

Figure 4 (a, b) represents the optical micrographs of the prepared sample (HT) with 1 wt. % Sn as a solid lubricant and 10 wt. % natural minerals as reinforcements. Abis ***et al.*** [35] have discussed the refinement of Si due to Sn addition because of the lower solubility of Sn in Al and the considerable difference in respective melting points so that it can get quickly filled inside the surface pores during sliding over the counter surface. Also, Sn atoms have more binding energy with vacancy due to their sizeable atomic size. These vacancies enhance the diffusion of eutectic-Si all over the matrix [36]. This helps in refining the Si, which can see in Figure 4a. An optical micrograph supports the above statement with smaller primary silicon (Figure 4b). Since reinforced particles and Sn can not be distinguished in the optical micrograph, a respective EDS line profile of the SEM image has also been taken, as shown in Figure 4c and d. The bright phase represents the presence of Sn. The lower melting point of Sn compared to Al covers the reinforcement in a liquid state, as shown in figure 4c. Further, Sn has refined the silicon (figure 4a) to an appreciable extent compared to unlubricated samples (figure 3a).

Figure 5(a, b) exhibits the microstructure of sample HG, which shows 1 wt. % self-lubricating Gr particles, which helps refine the primary silicon morphology. Graphite particles act as the nucleus to provide a solidification site for the remaining mass. Graphite particles were poured into the vortex formed in liquid during the mechanical stirring. By the string action, graphite particles overcome the surface energy barriers due to poor wettability of graphite with LM30 (Al-Si) alloy and the local shear force exerted on the bulk Gr agglomerates breaks the bulk cohesive graphite powder leading theirs to a uniform distribution in the matrix [37], [38]. Graphite particles form the glaze film on the pin surface during the sliding motion and reduce the apparent contact area. Figure 5c and d show the EDS line profile of the SEM image of the HG sample to investigate the presence of Gr particles.

Figure 6(a, b) represents the microstructure of the HTG sample, which is the mixture of (0.5 wt. % Gr + 0.5 wt. % Sn) with 10 wt. % (sillimanite + ilmenite). The microstructure reveals the presence of primary faceted Si and needle type eutectic Si having refined structure as compared to other composites. Since the reinforcement particles (sillimanite + ilmenite) and graphite particles have a high melting point so it provides more number of nucleation sites. Higher nucleation sites lead to the hindrance for the growth of primary silicon. Sillimanite, ilmenite, and graphite all restricted the growth of silicon primary phase and help to generate refined structure, which further helps in improved mechanical properties of

composites [39]. The EDS line profile of the SEM image of HTG sample is shown in Figure 6c and d. The presence of both tin and graphite as a solid lubricant can be seen.

3.2 Density

Figure 7a represents the comparative study of theoretical densities (ρ_{th}) and experimental density (ρ_{ex}), respectively. The graph shows the marginal difference between the ρ_{th} and ρ_{ex} of the synthesized composite. Moreover, ρ_{th} and ρ_{ex} densities of the composite are more than the B1 sample. It was due to incorporating a higher density of ilmenite + sillimanite particles than the base alloy. The study of Figure 7b reveals that the overall ρ_{th} of the formulated composites is less than commercial cast iron (C) material. It was demonstrated that the ρ_{th} of formulated composite HTG was ~60 % less than automobile grade cast iron density.

3.3 Hardness

3.3.1 Micro-hardness

Figure 8a shows the variation in the Vickers hardness of the prepared composites at matrix (M), reinforcement particles (P), and interface (I) between the matrix and reinforcement. It is revealed from Figure 8a that the micro-hardness of the B1 sample increased with the incorporation of reinforcement (SIllimanite & ilmenite) particles. There are three distinct hardness zones for the composite, where low hardness was observed in the matrix zone. Next, the zone with the maximum hardness was the reinforced particles, and the zone where the hardness value lay between the particle and the matrix was named the interfacial zone. The high hardness values at the particle-matrix interface represent the excellent bonding of particles with the matrix.

The Vickers hardness of the HT and HTG composite was ~ 4% and ~15%, more than the H1 sample, respectively. The cause of this is the refinement in microstructure with strong interfacial bonding between particles and matrix [39]. Thus, the processing route followed for the fabrication of the composites was adequate to achieve sound composites. However, the micro-hardness of HG sample showed a minimal increment ~ 3% than the other prepared composite, which was due to the addition of soft Gr particles. Gr particles have eased the movement of grains besides the slip planes and could lead to large deformation of material [40].

3.3.2 Bulk hardness

Figure 9b represents the bulk hardness of B1, composite, and commercial cast iron samples at the scale of B. It can be observed from the graphical data that the Rockwell hardness of prepared composite is increase by the addition of reinforcement (sillimanite & ilmenite) particles. It is also observed that the hardness of HG sample declines due to the incorporation of Gr soft particles. The HTG sample exhibited a ~44% increment in the Rockwell hardness than the B1 sample. Moreover, the Rockwell hardness of the HTG sample is ~7 % less as comparisons to cast iron (CI). The addition of the sillimanite and ilmenite

minerals increases the dislocation density of the composites. The increase in the dislocation density of the composites increases the hardness of the composites.

3.4 Wear analysis

3.4.1 Effect of sliding distance and applied load on the wear losses

Figure 9 (a-e) exhibits the variation in wear rate of different samples with sliding distance. For the base alloy and the composites, a similar trend in the wear results was observed. Figure 9 exhibits the two distinct zones *viz.* run-in wear (up to 1500m) and steady-state wear (1500-3000m). Initially, the wear rate of fabricated samples is higher up to the 250 m sliding distance. The initial increase in the wear rate of the samples is attributed to the asperity-to-asperity contact. Applying shear forces during sliding the cutting and plowing action of the sharp asperities of matrix in contact with the counter surface generates debris till 250m sliding distance [34,35], reflecting the abrasive wear nature during the relative motion.

Beyond the sliding distance of 250 m wear rate decreases, the continuous sliding increases the contact temperature and leads to the formation of oxides on the pin surface. The oxides decrease the relative area of contact between the pin and disc. Hence, a decrease in the wear rate is observed.

Next, in steady-state wear zone, the smaller debris was embedded between the counter surface and pin surface valleys. Now, the wear mechanism is converted from a two-body wear mechanism into a three-body wear mechanism. During continuous sliding, the contact temperature increases in the initial stage and after that wear is little increased. In this period, the pin's surface gets oxidized and forms a thermal barrier between pin and counter surface, preventing the contact pin subsurface from leading to reduced wear loss [37, 39].

Figure 10 (a, b) represents the comparative study of maximum wear rate and average wear rate of all samples, respectively, at different applied loads (9.81-68.67N). The average wear rate of LM30 (Al-Si) alloy and synthesized composites increases with the applied load. Higher applied load increases the frictional heating between the pin and the counter surface. This increases the contact temperature and causes softening of the pin surface and removing the oxidized area of the pin. This exposes new areas to wear. In addition, the counter surfaces get welded to the disc surface, tearing the pin surface and increasing wear rate. Also, higher load exhibited higher content of plastic deformation, resulting in higher wear loss. The material removal induced the delamination (severe fracture of the interface), forming micro-cracks and micro-plowing due to the application of shear force on the sub-surface during sliding motion [33, 36–39].

3.4.2 Effect of the reinforcement and lubricating material

Figure 10(a, b) represents the effect of reinforcement particles (sillimanite + ilmenite) on the average steady-state wear of the B1 sample and HAMCs (H1). As a result of the incorporation of the natural mineral(s) inside the metallic LM30 matrix, the wear loss has been reduced by ~37 % and ~ 29 % at lower load (9.81N) and higher load (68.67N). Generally, the observed wear behavior is associated with the

presence of ceramics phase's in the matrix. Moreover, some of the research groups have also suggested the influence of the re-distribution of Si inside the Al matrix that causes less wear losses as Si is hard phase (Figure 3a) [49].

The wear rate of the samples decreased with the incorporation of sillimanite and ilmenite particles. This was attributed to the fact that at given applied load, sillimanite and ilmenite particles bear a major portion of the applied load. The strong interfacial bonding keeps the particles stable and bonded to the matrix and hence, carries a major portion of applied load. Sillimanite and ilmenite particles protrude from the matrix and hold a significant portion of the applied load. The ceramics particles shield the matrix from deformation. Due to the continuous deformation, when one particle is fractured, the load is transferred to the other particles. Thus, further enhancement in the wear resistance is observed. Therefore the outcome is the reduced wear rate [46, 47].

To investigate the effect of solid lubricant (Sn and Gr) on wear performance of natural mineral reinforced Al-alloy composite, tin (Sn), graphite (Gr), and both were reinforced in the LM30 matrix with reinforcement minerals during the casting process. As a result, both components (Sn or Gr) exhibited their presence in the metallic (LM30) matrix, as shown in Figure 9c & d, respectively. Here, Figure 10b depicts the effect of solid lubricant (Sn/Gr/both) on the average steady-state wear rate on cast composites. As a result of the addition of solid lubricant(s), overall steady-state wear resistance has been increased up to ~ 3 % (at 9.81N) and ~ 24 % (at 68.67N) as compared to composites without solid lubricant(s).

In Gr-reinforced (1.0 wt%) composite samples (HG), a decrement of ~12 % has been observed at 9.81N, while ~14 % has occurred at 68.67N. The observed variation might be associated with the layered hexagonal structure of graphite and resulted in graphitized tribo- film along with Al-oxide film during the relative motion between pin and counter material [45, 46]. Due to the formation of a lubricating film which may behave like a barrier between asperities of pin and counter surface, it reduces the coefficient of friction and hence, reduces the shear stress between contact surfaces and enhances the wear resistance [54]–[57]

Similarly, Sn- reinforced (1.0 wt%) composite samples (HT10) reduced the wear rate ~11 % at 9.81N and ~41% at 68.67N, respectively. The observed decreased wear loss can be asserted to two significant factors that are (i) formation of Sn-oxide layer on the surface of the pin and (ii) melting of Sn due to frictional motion between pin and counter disc. Latter resulted in filling the asperities with molten Sn, which may further support the formation of the Sn-oxide layer and reduce seizure wear [58]. Moreover, Figure 10 also revealed the enhanced wear resistance of dual lubricant reinforced composite samples (HTG) with ~52 % at 9.81N and ~39 % at 68.67N compared to individual lubricant (Gr or Sn) composite samples. During the relative motion between the pin and counter surface, the combination of Sn and Gr resulted in the formation of lubricating film and oxide film, which enhanced the wear resistance [27].

Further, Figure 11 shows the comparative wear behavior study of cast iron (C) and HTG sample. Sample HTG exhibited ~6% less wear resistance as compared to cast iron. But, a lower density of aluminum

enables its applicability as brake rotors [59]. Thus, the observed results suggested that the HAMCs alternate against the cast iron for industrial revolution changes.

3.5 Coefficient of friction

The study of coefficient of friction (COF) of the B1 sample and synthesized composite at various loads (9.81-68.67 N) is shown in Figure 12. The graph trend is similar for all the samples, where it initially increases up to the applied load of 29.43 N, and after that, a decrease in COF is observed. For low load, less frictional heating is generated between the contact surfaces; thus, the COF at low applied load is less. For the low load (9.81 N), the COF of the B1, H1, HT, HG, and HTG samples was observed to be 0.55, 0.42, 0.29, 0.32, and 0.20, respectively. After that, the frictional heating increases with increasing the load. Therefore, an increment in the COF is also observed (Figure 12). For the applied load of 29.43 N, the COF of the B1, H1, HT, HG, and HTG samples was observed to be 0.76, 0.62, 0.55, 0.59, and 0.52, respectively. The COF is increased till the applied load of 29.43 N, beyond which the decrease in the COF is observed. For the applied load of 49.05 N, the COF of the B1, H1, HT, HG, and HTG samples was observed to be 0.73, 0.60, 0.52, 0.54, and 0.50, respectively. This declination in COF could be due to the more stable oxides layer on the pin surface. The increased frictional heating leads to forming an oxide layer on the pin surface and protects the surface from sliding contact, hence lesser the COF of the samples. Also, the higher applied loads, i.e., up to 49 N, leads to the formation of MML, which inhibits metal to metal contact and lowers the COF of the composites. For the high applied load of 68.67 N, the COF of the B1, H1, HT, HG, and HTG sample was observed to be 0.64, 0.52, 0.45, 0.47, and 0.42, respectively The incorporation of solid lubricating ingredients has a significant effect on the COF of the samples. The COF of the HT sample was lesser than the HG sample. The lowest COF was observed for the HGT sample (Figure 12).

3.6 Track and debris analysis

Figure 13 (a, b) shows the SEM image of worn tracks of the HTG sample at 9.81 N and 68.67 N load, respectively. The SEM images exhibit the grooves mark parallel in the direction of relative motion on the sample surface with some delamination mark. At the low load of 9.81 N, these narrow grooves on the sample lead to the abrasion wear between the contact surfaces. A few debris was also observed on the pin surface. Due to continuous sliding, some debris gets embedded into the soft matrix material.

Moreover, wider grooves were observed under the action of the high applied load. The asperities become wider and deformed in the direction of sliding, while the size of the asperities increases with the increase of the applied load up to 68.67 N (Figure 13b). Also, during the sliding material starts higher plastic deformation under the action of shear stress. This leads to the formation of microcracks and material losses in the form of debris as delamination of the sample surface (Figure 13b) [50], [52]–[55], [59]. This represents that for 68.67N load, the material removal is the adhesive wear nature. In this order, small debris is also seen on the wear track due to the continuous motion. Due to the combined action of applied load and constant sliding speed, the debris gets embedded in the wear tracks of the pin surface (Figure 13b). The HAMC surface had undergone mild zwear, which can be attributed to the oxidative wear mechanism. Oxide layers were formed on the surface of the composite as the pin scratches away some

of the surface material. This oxide layer restricts further removal of material by limiting the formation of the transfer layer.

Figures 13c and 13d present the SEM images of wear debris of the HTG sample at an applied load of 9.81 N and 68.67 N, respectively. Majorly flake-like debris was observed. Flake-like debris is formed as a result of delamination. The continuous sliding leads to the plastic deformation of the pin surface and leads to microcracks. When microcracks meet with each other, they lead to the removal of material in the form of flakes, leading to the formation of flake-like debris [60]. Grooves on debris are also visible. The debris's grooves indicate micro plowing action during the initial run-in wear zone [32]. The presence of grooves on debris reveals that initially, abrasive wear was dominant [33].

Further, a few small-sized wear debris are attached to the wear surface, which signifies the continuous removal of debris from their surface [20]. These wear debris reduced the wear rate of the composite by avoiding the exposure of soft matrix material to the steel counter surface. As sliding distance increases, crack formation followed by material removal in the form of flakes has occurred by leaving a crater behind it. The presence of microcracks on the wear debris represents the plastic deformation of the working surface due to the application of shear force on the subsurface during sliding motion.

Figure 14 represents the EDS analysis of the HTG wear track at a 68.67 N applied load. Spectrum peaks are observed for various elements like Al, Cu, Fe, Ti, O. The presence of oxygen proves that the formation of aluminum oxide, iron oxide, and silicon oxide during wear. The source of iron is the counter surface. Due to the continuous sliding at higher applied load leads to debris formation from the pin surface. This debris gets trapped between the pin and the counter surface and prevents direct metal-to-metal contact of pin and disc. The debris of the pin surface and the counter surface gets compacted between the pin and the disc and begin to flow/roll in the direction of sliding. The possibility of accumulation of wear debris at the valleys between protruded corundum particles is higher for the composites than the base alloy. As a result, higher counter surface material gets transferred and finally accommodated as MML on the composite surface and increases the wear resistance of the prepared composites. Figure 14b and 14c present the EDS analysis of ASGT10 wear debris at a load of 68.67 N. The spectrum of the debris shows peaks of different elements like Al, Cu, Fe, and O. Further, the presence of Sn and carbon in the wear debris indicate their role as solid lubricants. These lubricating agents compliment the wear resistance and provide superior wear resistance to the composites.

4. Conclusions

The influence of solid lubricant on the wear properties of synthesized composites has been studied. Some significant studies are given below:

- Optical micrographs show the presence of uniformly distributed reinforced particles throughout the matrix. Other solid lubricants viz. Sn and Gr were homogeneously distributed throughout the matrix. Also, the addition of ceramic particles refined the primary and eutectic silicon morphology.

- Vickers hardness study revealed high hardness values at the particle-matrix interface, indicating strong interfacial bonding of particles with the matrix. Further, Rockwell hardness showed that the hardness of the composites improved with the addition of reinforcement and the best hardness was observed with both Sn and Gr.
- The addition of solid lubricants decreased the wear rate and coefficient of friction of the composites. Best wear results were observed for the composites with both Sn and Gr.
- SEM analysis shows that at a low load of 9.81 N, the abrasive wear mechanism was dominant. The high load of 68.67 N adhesive wear mechanism was dominant for material removal. Further, EDS analysis indicates the formation of various oxides on the pin surface and wear debris, indicating an oxide layer and mechanically mixed layer on the pin surface.
- The wear rate of the composites was comparable to the cast iron. Moreover, the composites have a lower density than the cast iron. Thus, for industrial applications like brake rotors, composites provide a significant weight reduction over the conventional cast-iron material.

Declarations

Consent to participate

Authors does not performed any studies involving human or animal participation.

Consent for publication

Consent was got from all individual authors included in the study to publish data.

Availability of Data and Material

All the data and material incorporated in the present manuscript will be made available whenever required.

Acknowledgment

Author (VS) thanks Dr. Aayush Gupta for valuable suggestions in drafting the manuscript.

Author's contribution

Varun Singhal: Conceptualization, design of study, data optimization, analysis, manuscript writing. **O. P. Pandey:** Results analysis, manuscript writing.

Disclosure of potential conflict of interest

Authors do not have any conflict of interest

Compliance with ethical standards

Formal consent is not compulsory for the above type of work.

Funding Details

The authors did not receive any financial support from any funding agency

References

[1] P. Rohatgi, “Cast aluminum-matrix composites for automotive applications,” *Jom*, vol. 43, no. 4, pp. 10–15, 1991.

[2] T. Garg, P. Mathur, V. Singhal, C. Jain, and P. Gupta, “Underwater Friction Stir Welding: An Overview,” *International Review of Applied Engineering Research*, vol. 4, no. 2, pp. 2248–9967, 2014.

[3] S. Kumar, V. Sharma, R. S. Panwar, and O. P. Pandey, “Wear behavior of dual particle size (DPS) zircon sand reinforced aluminum alloy,” *Tribology Letters*, vol. 47, no. 2, pp. 231–251, 2012.

[4] M. Maurya, S. Kumar, and V. Bajpai, “Assessment of the mechanical properties of aluminium metal matrix composite: A review,” *Journal of Reinforced Plastics and Composites*, vol. 38, no. 6, pp. 267–298, 2019.

[5] S. C. Tjong, *Processing and Deformation Characteristics of Metals Reinforced with Ceramic Nanoparticles*. 2013.

[6] J. J. Rino, D. Chandramohan, and V. D. Jebin, “RESEARCH REVIEW ON CORROSION BEHAVIOUR OF METAL MATRIX COMPOSITES.”

[7] N. Radhika and R. Raghu, “Abrasive wear behavior of monolithic alloy, homogeneous and functionally graded aluminum (LM25/AlN and LM25/SiO2) composites,” *Particulate Science and Technology*, vol. 37, no. 1, pp. 10–20, 2019.

[8] G. B. V. Kumar, R. Pramod, C. G. Sekhar, G. P. Kumar, and T. Bhanumurthy, “Investigation of physical, mechanical and tribological properties of Al6061–ZrO2 nano-composites,” *Heliyon*, vol. 5, no. 11, pp. 0–7, 2019.

[9] M. Singla, D. D. Dwivedi, L. Singh, and V. Chawla, “Development of Aluminium Based Silicon Carbide Particulate Metal Matrix Composite,” *Journal of Minerals and Materials Characterization and Engineering*, vol. 08, no. 06, pp. 455–467, 2015.

[10] A. Canakci and F. Arslan, “Abrasive wear behaviour of B4C particle reinforced Al2024 MMCs,” *International Journal of Advanced Manufacturing Technology*, vol. 63, no. 5–8, pp. 785–795, 2012.

[11] O. Yilmaz and S. Buytoz, “Abrasive wear of Al2O3-reinforced aluminium-based MMCs,” *Composites Science and Technology*, vol. 61, no. 16, pp. 2381–2392, 2001.

[12] M. O. Bodunrin, K. K. Alaneme, and L. H. Chown, “Aluminium matrix hybrid composites: A review of reinforcement philosophies; Mechanical, corrosion and tribological characteristics,” *Journal of Materials Research and Technology*, vol. 4, no. 4, pp. 434–445, 2015.

[13] H. Abdizadeh and M. A. Baghchesara, “Investigation into the mechanical properties and fracture behavior of A356 aluminum alloy-based ZrO2-particle-reinforced metal-matrix composites,” *Mechanics of Composite Materials*, vol. 49, no. 5, pp. 571–576, 2013.

[14] Zuhailawati H., P. Samayamutthirian, and Mohd Haizu C.H., “Fabrication of low cost of aluminium ,matrix composite reinforced with silica sand,” *Journal of Physical Science*, vol. 18, no. 1, pp. 47–55, 2007.

[15] R. Arora, S. Kumar, G. Singh, and O. P. Pandey, “Effect of applied pressure on the tribological behaviour of dual particle size rutile reinforced LM13 alloy composite,” in *Characterization of Minerals, Metals, and Materials 2015*, 2016, pp. 755–762.

[16] S. C. Sharma, “The sliding wear behavior of A16061-garnet particulate composites,” *Wear*, vol. 249, no. 12, pp. 1036–1045, 2001.

[17] S. Kumar, R. S. Panwar, and O. P. Pandey, “Tribological characteristics of aluminium tri-reinforced particles (Al- TRP) composites developed by liquid metallurgy route,” *Advanced Materials Research*, vol. 585, pp. 574–578, 2012.

[18] B. Vinod, S. Ramanathan, V. Ananthi, and N. Selvakumar, “Fabrication and characterization of organic and in-organic reinforced A356 Aluminium matrix hybrid composite by improved double-stir casting,” *Silicon*, vol. 11, no. 2, pp. 1–13, 2018.

[19] S. V Prasad and R. Asthana, “Aluminum metal – matrix composites for automotive applications : tribological considerations,” vol. 17, no. 3, 2004.

[20] S. Sharma, T. Nanda, and O. P. Pandey, “Effect of particle size on dry sliding wear behaviour of sillimanite reinforced aluminium matrix composites,” *Ceramics International*, vol. 44, no. 1, pp. 104–114, 2018.

[21] M. Singh, D. P. Mondal, A. K. Jha, S. Das, and A. H. Yegneswaran, “Preparation and properties of cast aluminium alloy–sillimanite particle composite,” *Composites Part A: Applied Science and Manufacturing*, vol. 32, no. 6, pp. 787–795, 2001.

[22] L. Rasidhar, A. R. Krishna, and C. S. Rao, “Fabrication and investigation on properties of Ilmenite (FeTiO3) based al-nanocomposite by stir casting process,” *International Journal of Bio-Science and Bio-Technology*, vol. 5, no. 4, pp. 193–199, 2013.

[23] A. Gupta, V. Singhal, and O. P. Pandey, “Facile in-situ synthesis of NbB 2 nanoparticles at low temperature,” *Journal of Alloys and Compounds*, vol. 736, pp. 306–313, 2018.

[24] M. Singh, D. P. Mondal, A. K. Jha, S. Das, and A. H. Yegneswaran, “Preparation and properties of cast aluminium alloy ± sillimanite particle composite,” vol. 32, pp. 787–795, 2001.

[25] R. Gupta, S. Sharma, T. Nanda, and O. P. Pandey, “Wear studies of hybrid AMCs reinforced with naturally occurring sillimanite and rutile ceramic particles for brake-rotor applications,” *Ceramics International*, vol. 46, no. 10, pp. 16849–16859, 2020.

[26] N. C. Kaushik and R. N. Rao, “Tribology International Effect of applied load and grit size on wear coef fi cients of Al 6082 – SiC – Gr hybrid composites under two body abrasion,” *Tribiology International*, vol. 103, pp. 298–308, 2016.

[27] S. Srivastava, S. Mohan, Y. Srivastava, and A. J. Shukla, “Study of the wear and friction behavior of immiscible as cast-Al- Sn / Graphite composite Abstract :,” *International Journal of Modern Engineering Research*, vol. 2, no. 2, pp. 25–42, 2012.

[28] E. Omrani, A. D. Moghadam, P. L. Menezes, and P. K. Rohatgi, “Influences of graphite reinforcement on the tribological properties of self-lubricating aluminum matrix composites for green tribology, sustainability, and energy efficiency—A review,” *International Journal of Advanced Manufacturing Technology*, vol. 83, no. 1–4, pp. 325–346, 2016.

[29] R. Tyagi, “Synthesis and tribological characterization of in situ cast Al-TiC composites,” *Wear*, vol. 259, no. 1–6, pp. 569–576, 2005.

[30] S. Das, S. V Prasad, and T. R. Ramachandran, “Microstructure and wear of cast (Al-Si alloy)-graphite composites,” *Wear*, vol. 133, pp. 173–187, 1989.

[31] S. Sharma, T. Nanda, and O. P. Pandey, “Effect of dual particle size (DPS) on dry sliding wear behaviour of LM30/sillimanite composites,” *Tribology International*, vol. 123, pp. 142–154, 2018.

[32] V. Sharma, S. Kumar, R. S. Panwar, and O. P. Pandey, “Microstructural and wear behavior of dual reinforced particle (DRP) aluminum alloy composite,” *Journal of Materials Science*, vol. 47, no. 18, pp. 6633–6646, 2012.

[33] V. Vijeesh and K. N. Prabhu, “Review of microstructure evolution in hypereutectic Al-Si alloys and its effect on wear properties,” *Transactions of the Indian Institute of Metals*, vol. 67, no. 1, pp. 1–18, 2014.

[34] J. Jorstad and D. Apelian, “Hypereutectic al-si alloys: Practical casting considerations,” *International Journal of Metalcasting*, vol. 3, no. 3, pp. 13–36, 2009.

[35] S. Abis, G. Barucca, and P. Mengucci, “Electron microscopy characterization of AlSn metal-metal matrix composites,” *Journal of Alloys and Compounds*, vol. 215, no. 1–2, pp. 309–313, 1994.

[36] B. T. Sofyan *et al.*, “Effects of Sn content on the characteristics of 319 aluminium alloy,” *Proceedings of the Australasian Conference and Exhibition - Aluminium Cast House Technology*, vol.

2005, pp. 161–168, 2005.

[37] D. Abdul Saheb, “Aluminum silicon carbide and aluminum graphite particulate composites,” *Journal of Engineering and Applied Sciences*, vol. 6, no. 10, pp. 41–46, 2011.

[38] P. Sharma, S. Sharma, and D. Khanduja, “Journal of Asian Ceramic Societies A study on microstructure of aluminium matrix composites,” *Integrative Medicine Research*, vol. 3, no. 3, pp. 240–244, 2015.

[39] S. Kumar, R. S. Panwar, and O. P. Pandey, “Effect of dual reinforced ceramic particles on high temperature tribological properties of aluminum composites,” *Ceramics International*, vol. 39, no. 6, pp. 6333–6342, 2013.

[40] K. H. W. Seah, S. c. Sharma, and B. m. Girish, “Mechanical particulate properties composites of cast ZA -27 / graphite particulate Composites,” *Materials & Design*, vol. 16, no. 5, pp. 1–5, 1995.

[41] M. M. Haque and A. Sharif, “Study on wear properties of aluminium – silicon piston alloy,” vol. 118, pp. 69–73, 2001.

[42] B. K. Show, D. K. Mondal, and J. Maity, “Dry Sliding Wear Behavior of Aluminum-Based Metal Matrix Composites with Single (Al2O3) and Hybrid (Al2O3+ SiC) Reinforcements,” *Metallography, Microstructure, and Analysis*, vol. 3, no. 1, pp. 11–29, 2014.

[43] A. Sharma, S. Kumar, G. Singh, and O. P. Pandey, “Effect of particle size on wear behavior of al-garnet composites,” *Particulate Science and Technology*, vol. 33, no. 3, pp. 234–239, 2015.

[44] R. N. Rao, S. Das, D. P. Mondal, and G. Dixit, “RETRACTED: Dry sliding wear behaviour of cast high strength aluminium alloy (Al–Zn–Mg) and hard particle composites,” *Wear*, vol. 267, no. 9–10, pp. 1688–1695, Sep. 2009.

[45] G. Ranganath, S. C. Sharma, and M. Krishna, “Dry sliding wear of garnet reinforced zinc / aluminium metal matrix composites,” vol. 251, pp. 1408–1413, 2001.

[46] J. Singh and A. C. Chauhan, “Overview of wear performance of aluminium matrix composites reinforced with ceramic materials under the influence of controllable variables,” *Ceramics International*, vol. 42, no. 1, pp. 56–81, 2015.

[47] T. Rajmohan, K. Palanikumar, and S. Ranganathan, “Evaluation of mechanical and wear properties of hybrid aluminium matrix composites,” *Transactions of Nonferrous Metals Society of China (English Edition)*, vol. 23, no. 9, pp. 2509–2517, 2013.

[48] K. Kaur and O. P. Pandey, “Microstructural characteristics of spray formed zircon sand reinforced LM13 composite,” *Journal of Alloys and Compounds*, vol. 503, no. 2, pp. 410–415, 2010.

[49] R. S. Panwar, S. Kumar, R. Pandey, and O. P. Pandey, “Study of non-lubricated wear of the Al-Si alloy composite reinforced with different ratios of coarse and fine size zircon sand particles at different ambient temperatures,” *Tribology Letters*, vol. 55, no. 1, pp. 83–92, 2014.

[50] S. Basavarajappa, G. Chandramohan, K. Mukund, M. Ashwin, and M. Prabu, “Dry Sliding Wear Behavior of Al 2219/SiCp-Gr Hybrid Metal Matrix Composites,” *Journal of Materials Engineering and Performance*, vol. 15, no. 6, pp. 668–674, Dec. 2006.

[51] S. C. Lim, “The relevance of wear-mechanism maps to mild-oxidational wear,” *Tribology International*, vol. 35, no. 11, pp. 717–723, 2002.

[52] T. S. Mahmoud, “Tribological behaviour of A390/Grp metal-matrix composites fabricated using a combination of rheocasting and squeeze casting techniques,” *Proceedings of the Institution of Mechanical Engineers, Part C: Journal of Mechanical Engineering Science*, vol. 222, no. 2, pp. 257–265, 2008.

[53] S. Doddamani, M. Kaleemulla, Y. Begum, A. KJ, and K. J. Anand, “An Investigation on Wear Behavior of Graphite Reinforced Aluminum Metal Matrix Composites,” pp. 1–6, 2017.

[54] C. S. Sivaramakrishnan, R. K. Mahanti, and R. Kumar, “The dispersion of lead and graphite in aluminium alloys for bearing applications,” *Wear*, vol. 96, no. 2, pp. 121–134, 1984.

[55] H. Torabian, J. P. Pathak, and S. N. Tiwari, “On wear characteristics of leaded aluminium-silicon alloys,” *Wear*, vol. 177, no. 1, pp. 47–54, 1994.

[56] S. Mahdavi and F. Akhlaghi, “Effect of the graphite content on the tribological behavior of Al/Gr and Al/30SiC/Gr composites processed by in situ powder metallurgy (IPM) method,” *Tribology Letters*, vol. 44, no. 1, pp. 1–12, 2011.

[57] A. Baradeswaran and A. Elaya Perumal, “Study on mechanical and wear properties of Al 7075/Al2O 3/graphite hybrid composites,” *Composites Part B: Engineering*, vol. 56, pp. 464–471, 2014.

[58] M. K. Surappa, “Aluminium matrix composites: Challenges and opportunities,” *Sadhana - Academy Proceedings in Engineering Sciences*, vol. 28, no. 1–2, pp. 319–334, 2003.

[59] R. Manikandan, T. V. Arjunan, and A. R. Akhil, “Studies on micro structural characteristics, mechanical and tribological behaviours of boron carbide and cow dung ash reinforced aluminium (Al 7075) hybrid metal matrix composite,” *Composites Part B: Engineering*, vol. 183, no. November 2019, 2020.

[60] S. Sharma, T. Nanda, and O. P. Pandey, “Investigation of T4 and T6 heat treatment on the wear properties of sillimanite reinforced LM30 aluminium alloy composites,” *Wear*, vol. 426–427, no. December 2018, pp. 27–36, 2019.

Figures

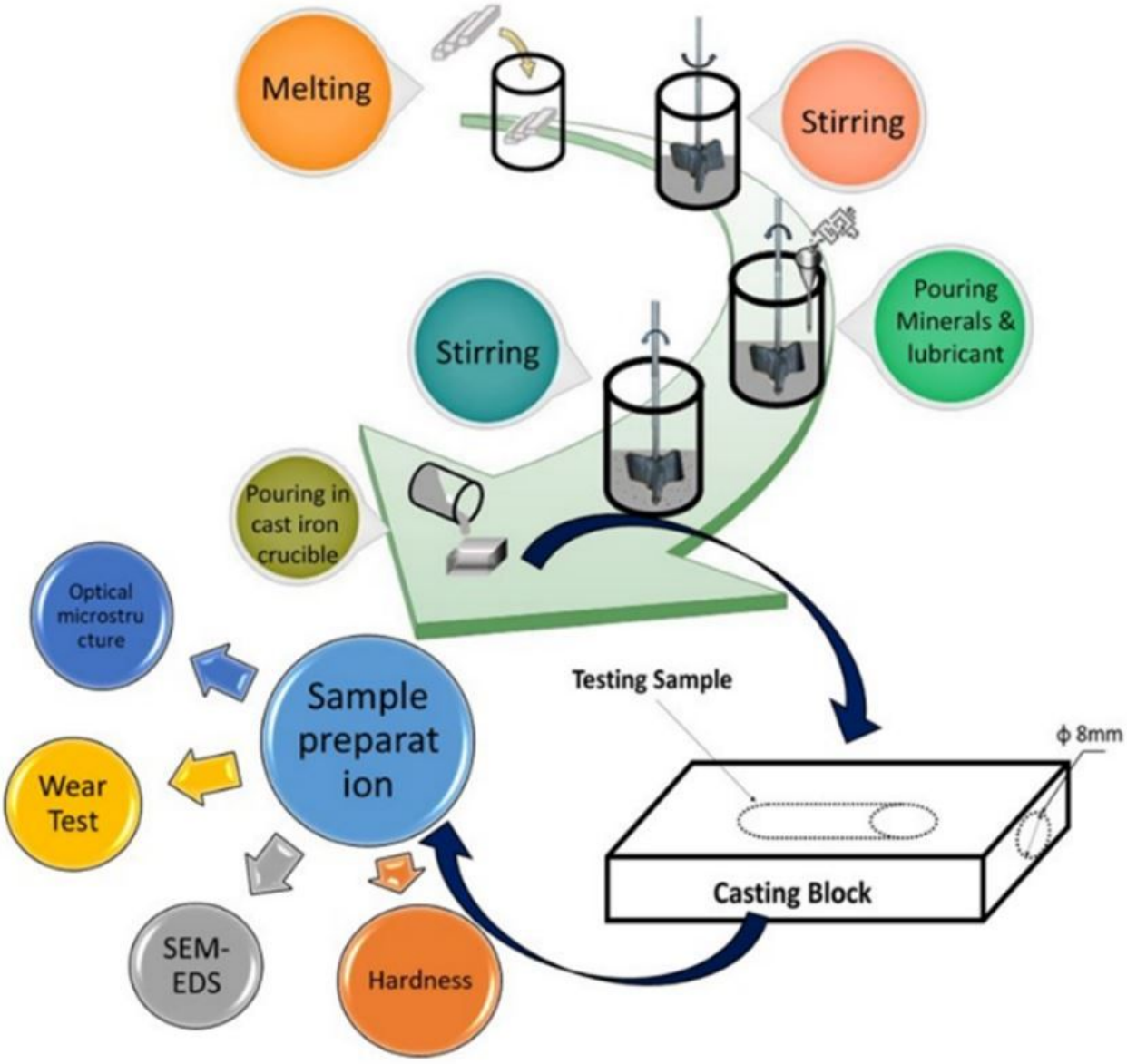

Figure 1

Represents the steps adopted for synthesizing and testing the HAMCs in the present work.

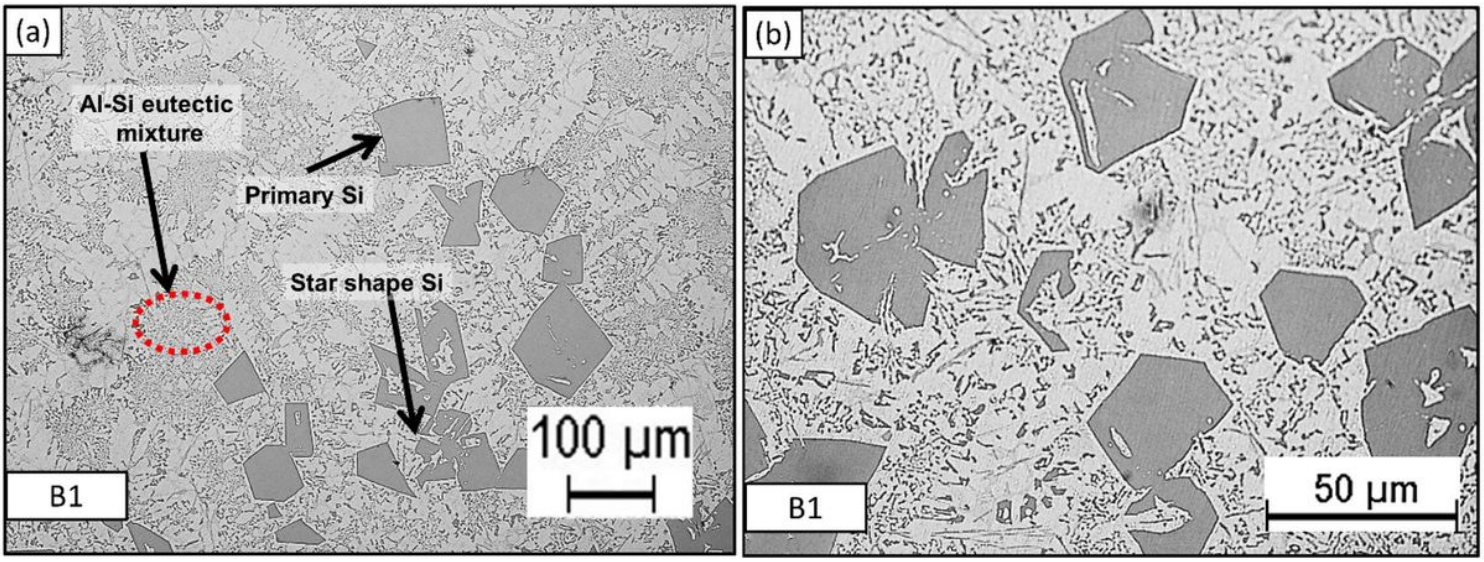

Figure 2

Represents the microstructure of as-cast base alloy (LM 30) at (a) 100 X and (b) 500X magnification.

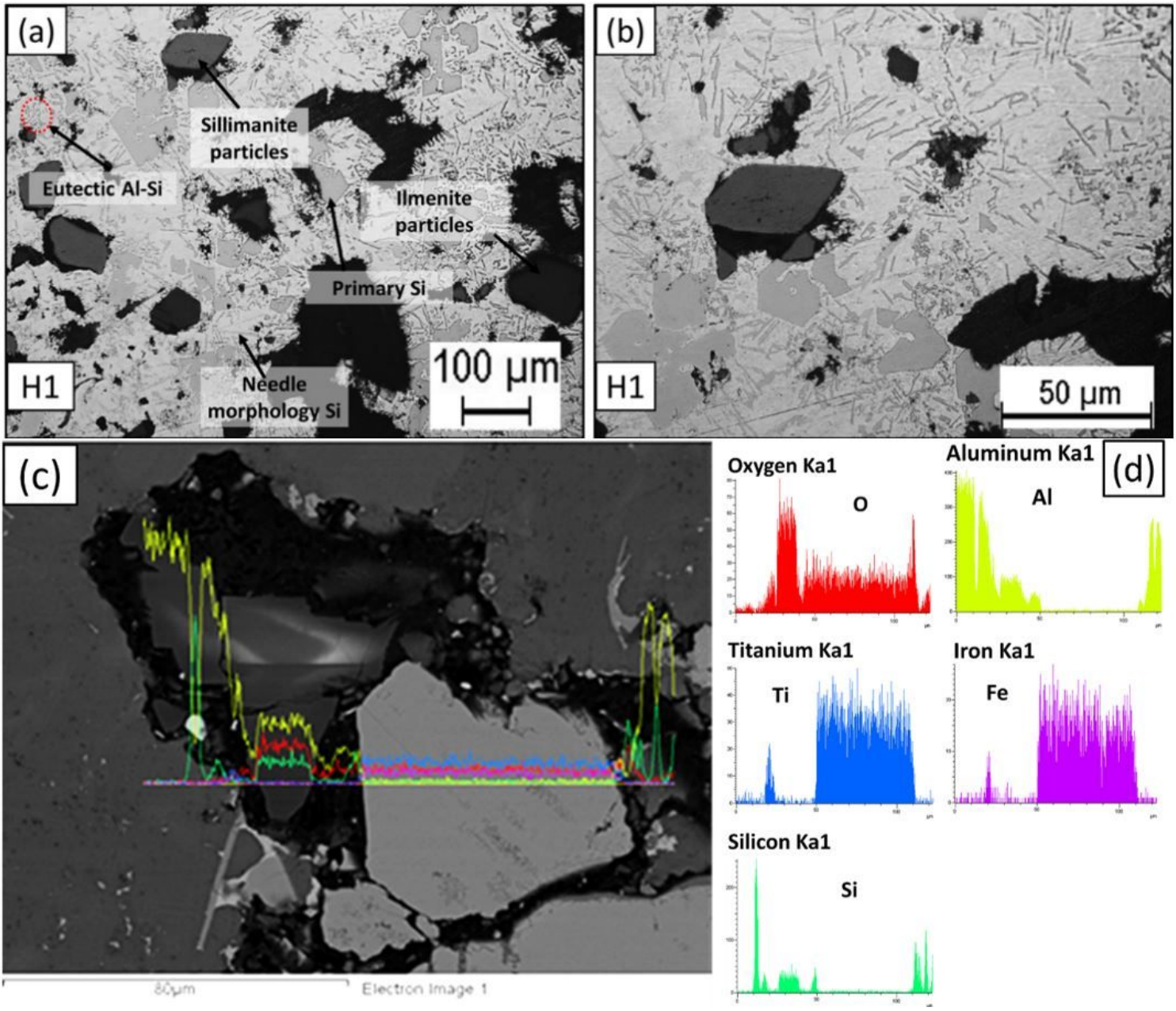

Figure 3

Represent the micrograph of 1 wt. % (sillimanite & ilmenite) reinforced composite at (a) 100 X, (b) 500X magnification, and (c & d) EDS line profile of SEM image of H1 sample.

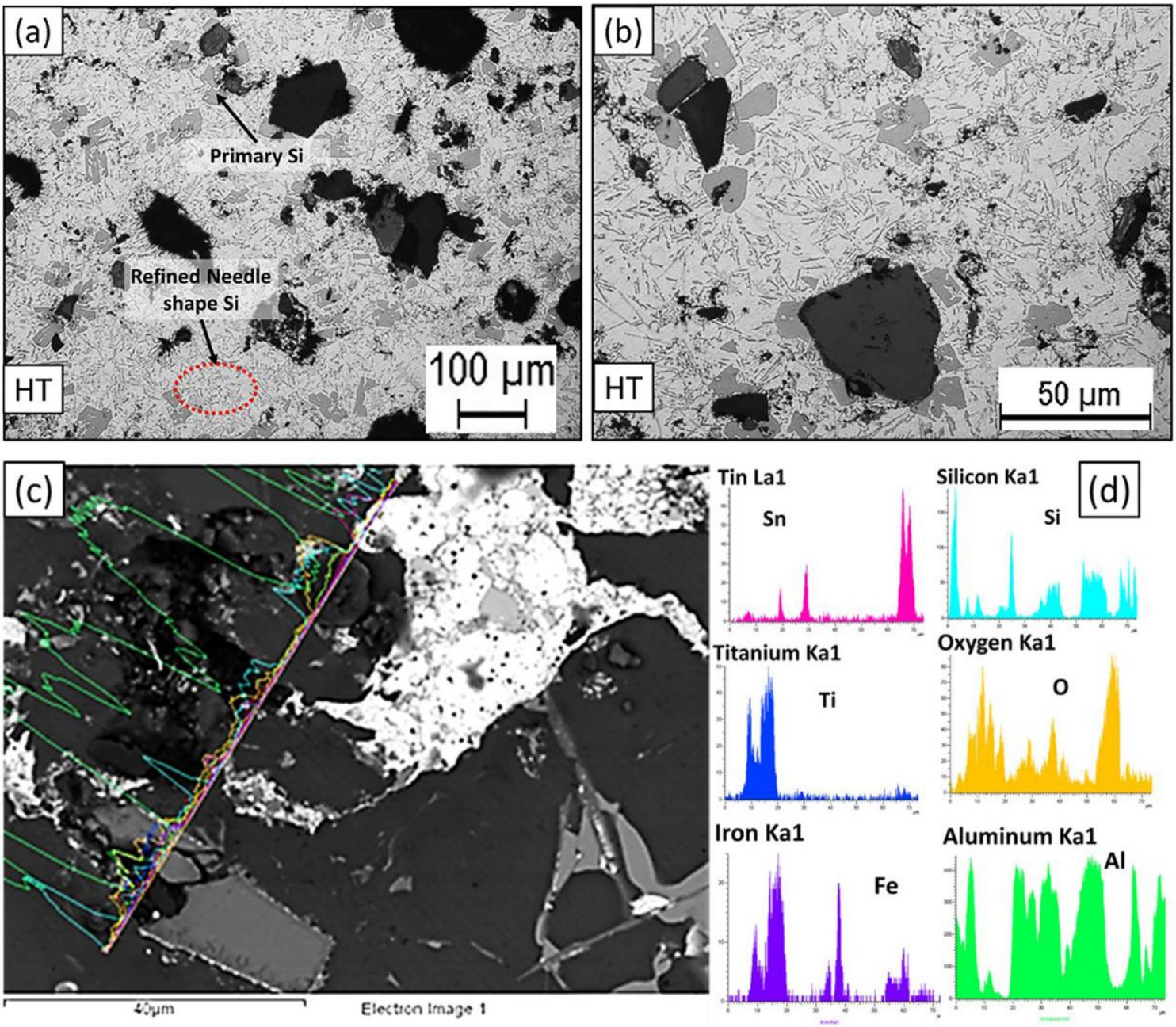

Figure 4

Represent the micrograph of 1 wt. % (sillimanite & ilmenite) reinforced composite with 1 wt. % Sn at (a) 100 X, (b) 500X magnification, and (c & d) EDS line profile of SEM image of HT sample.

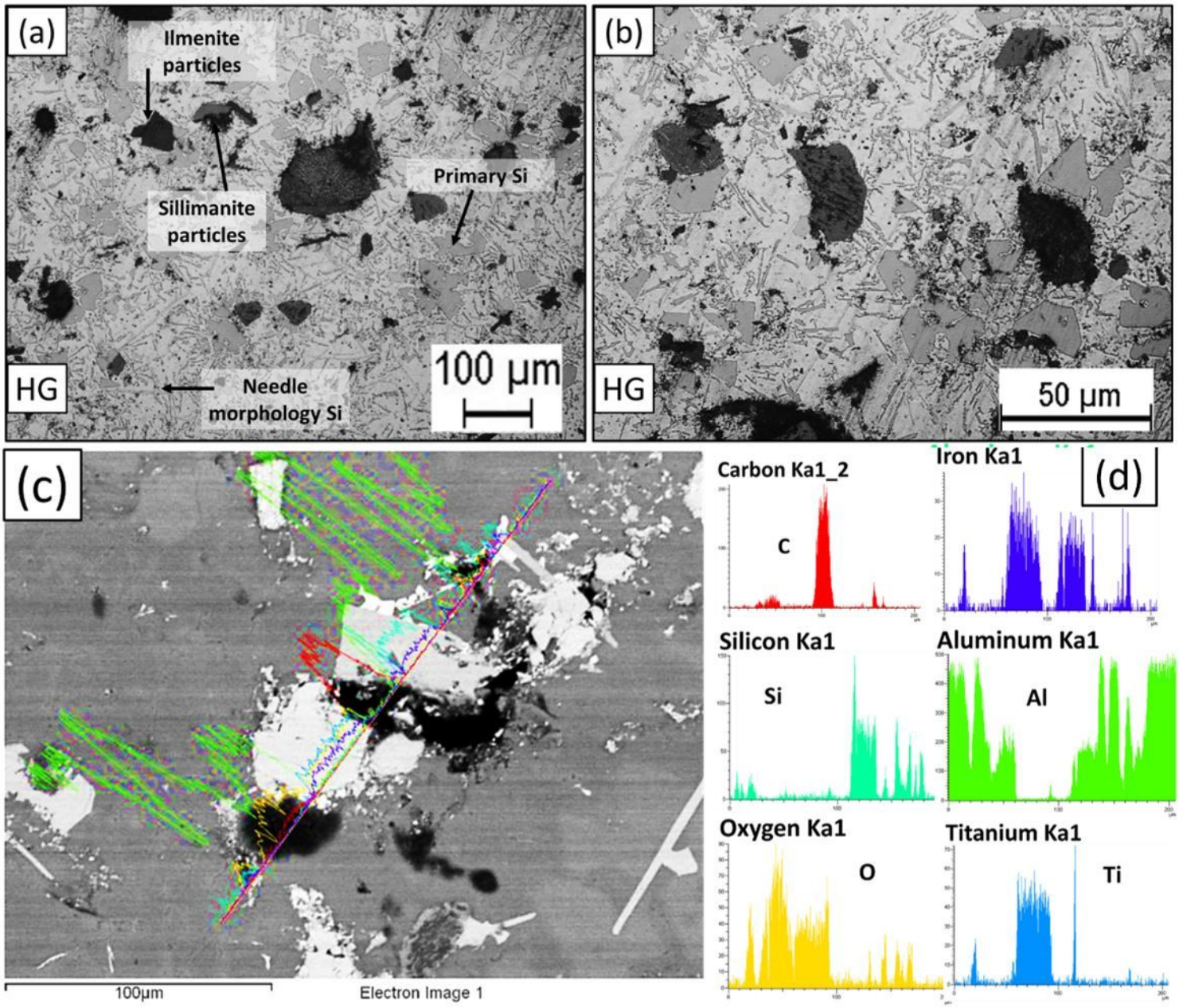

Figure 5

Represent the micrograph of 1 wt. % (sillimanite & ilmenite) reinforced composite with 1 wt. % Gr at (a) 100 X, (b) 500X magnification, and (c & d) EDS line profile of SEM image of H1 sample.

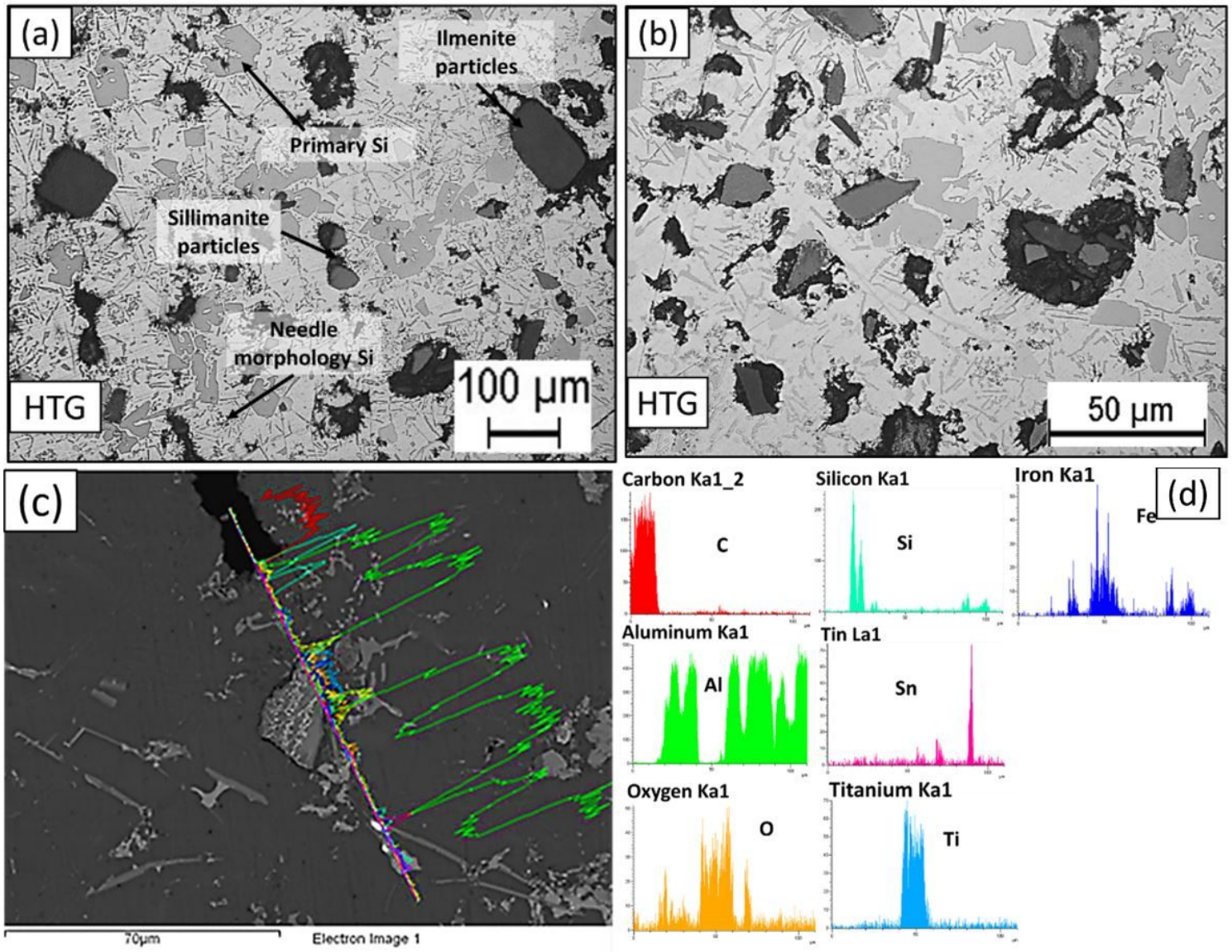

Figure 6

Represent the micrograph of 1 wt. % (sillimanite & ilmenite) reinforced composite with 1 wt. % (Sn + Gr) at (a) 100 X, (b) 500X magnification and (c & d) EDS line profile of SEM image of HTG sample.

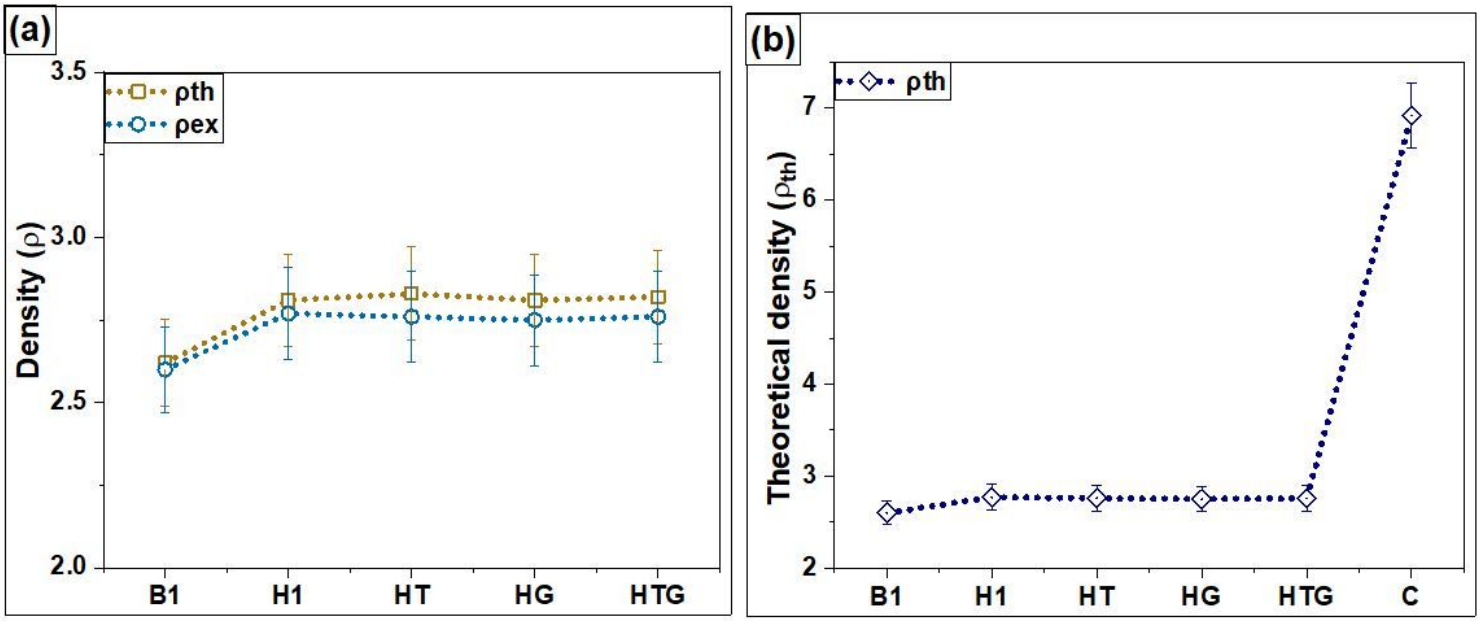

Figure 7

(a) Comparison study of ρth and ρex of synthesized composites, (b) ρth of synthesized composites and cast iron.

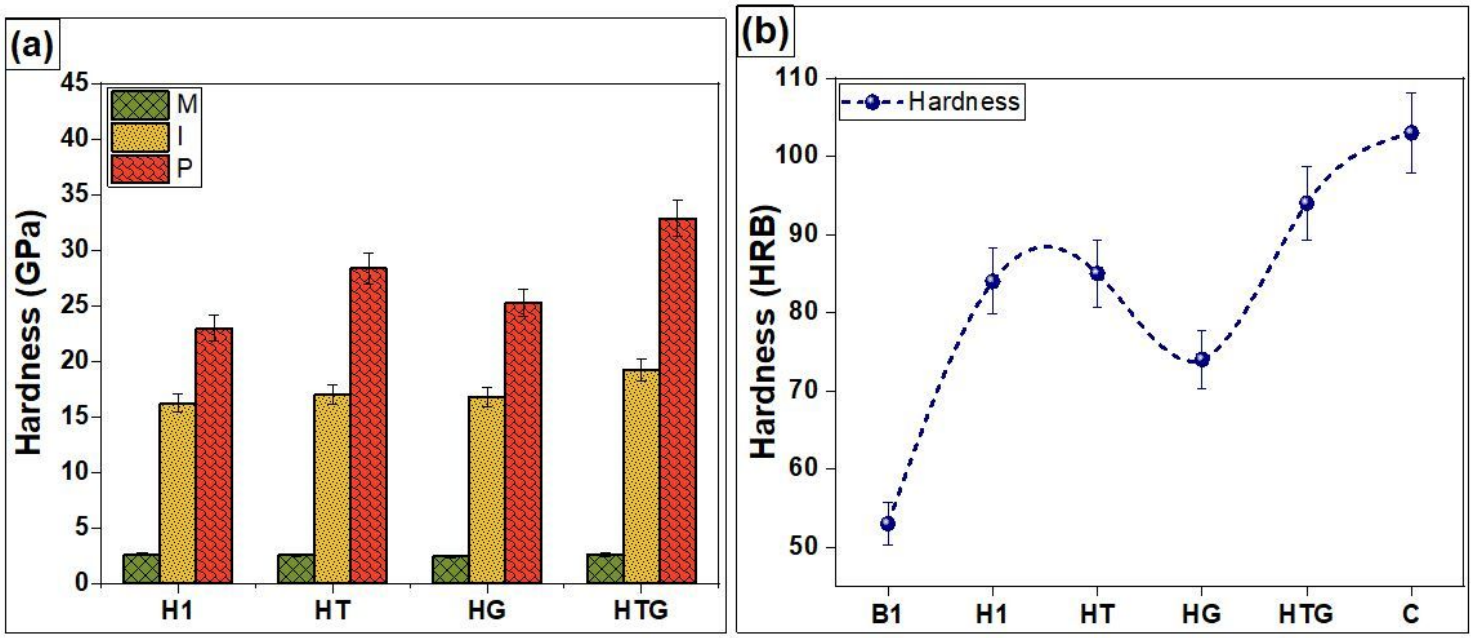

Figure 8

(a) Represent the Vickers-hardness of formulated samples, (b) Rockwell hardness values of prepared samples and cast iron.

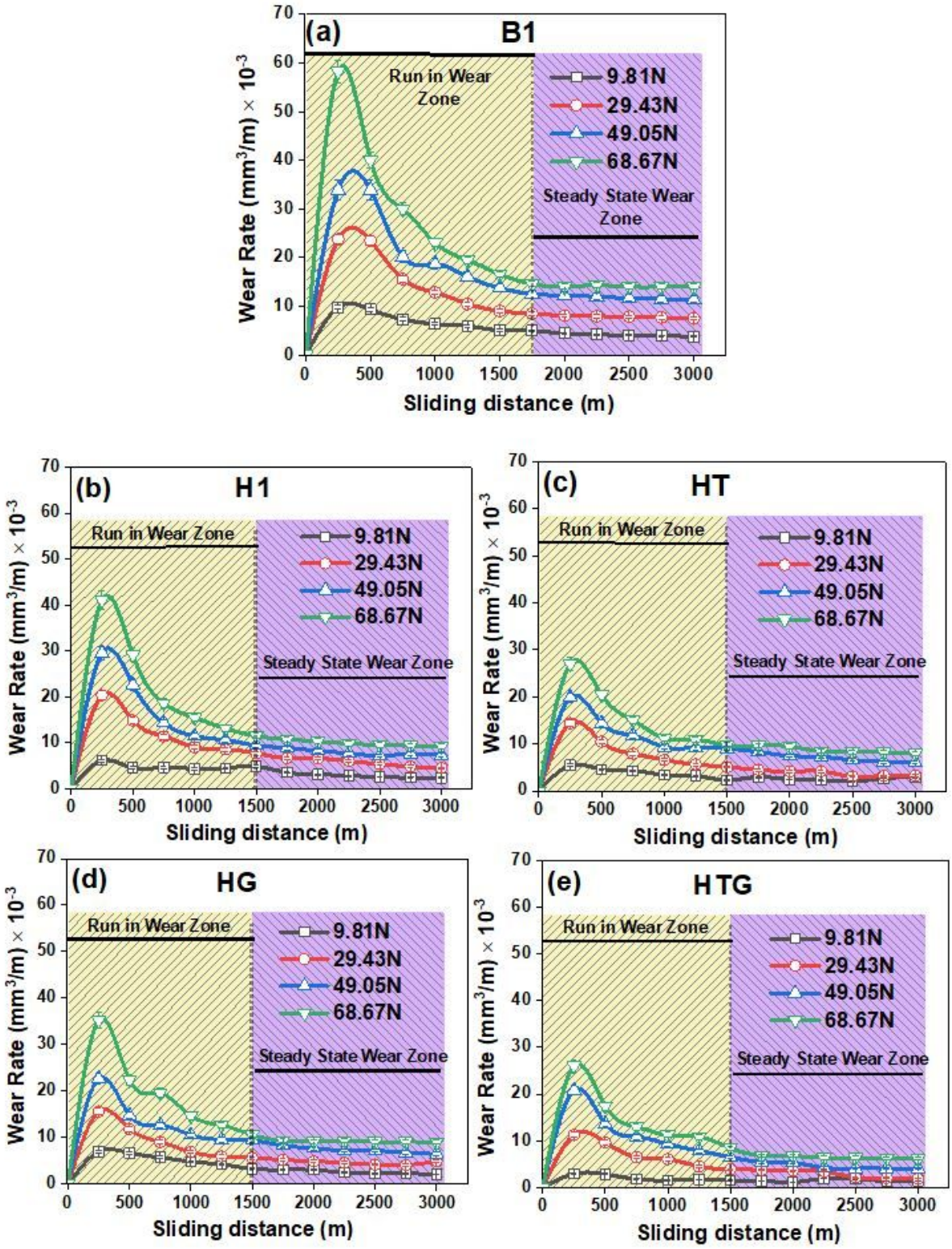

Figure 9

Representative wear behavior of (a) Base alloy and (b-e) Formulated composite showing run in and steady-state wear at different load (9.81-68.67 N).

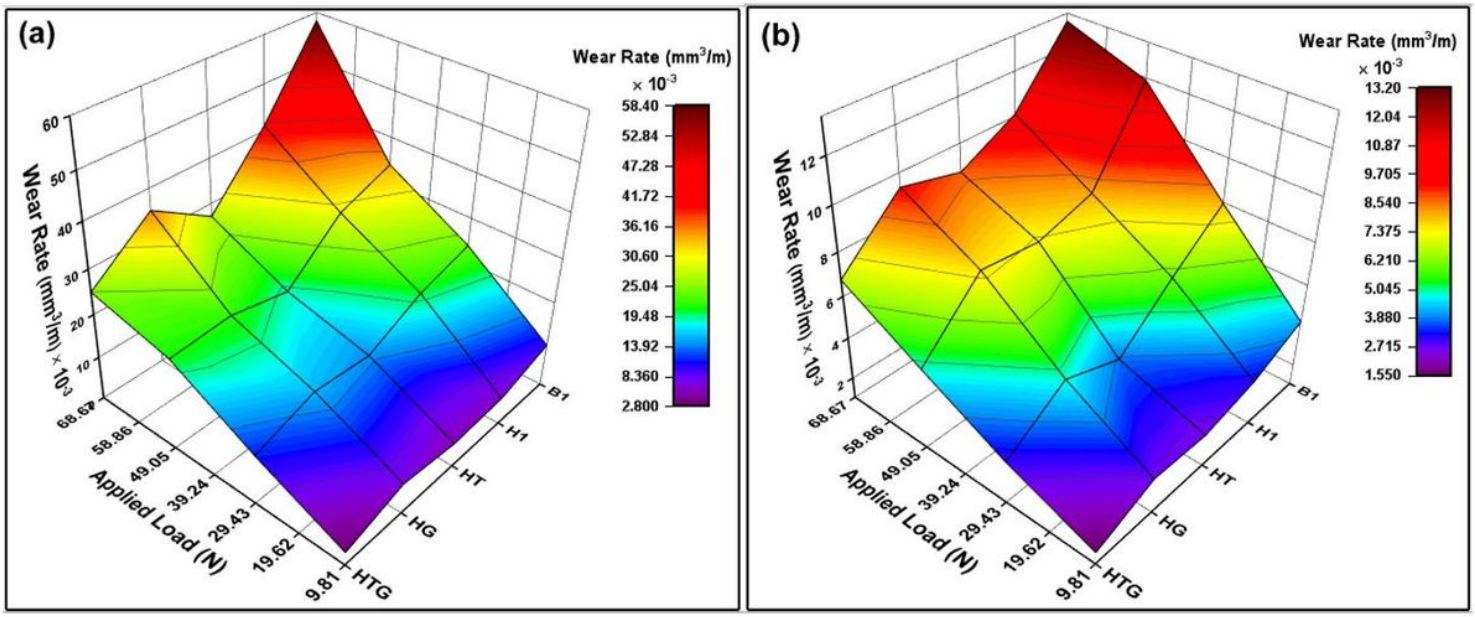

Figure 10

Represents the study of dry sliding wear behavior of B1 and various formulated samples (a) Maximum wear rate and (b) Average steady-state wear at 9.81-68.67N applied loads.

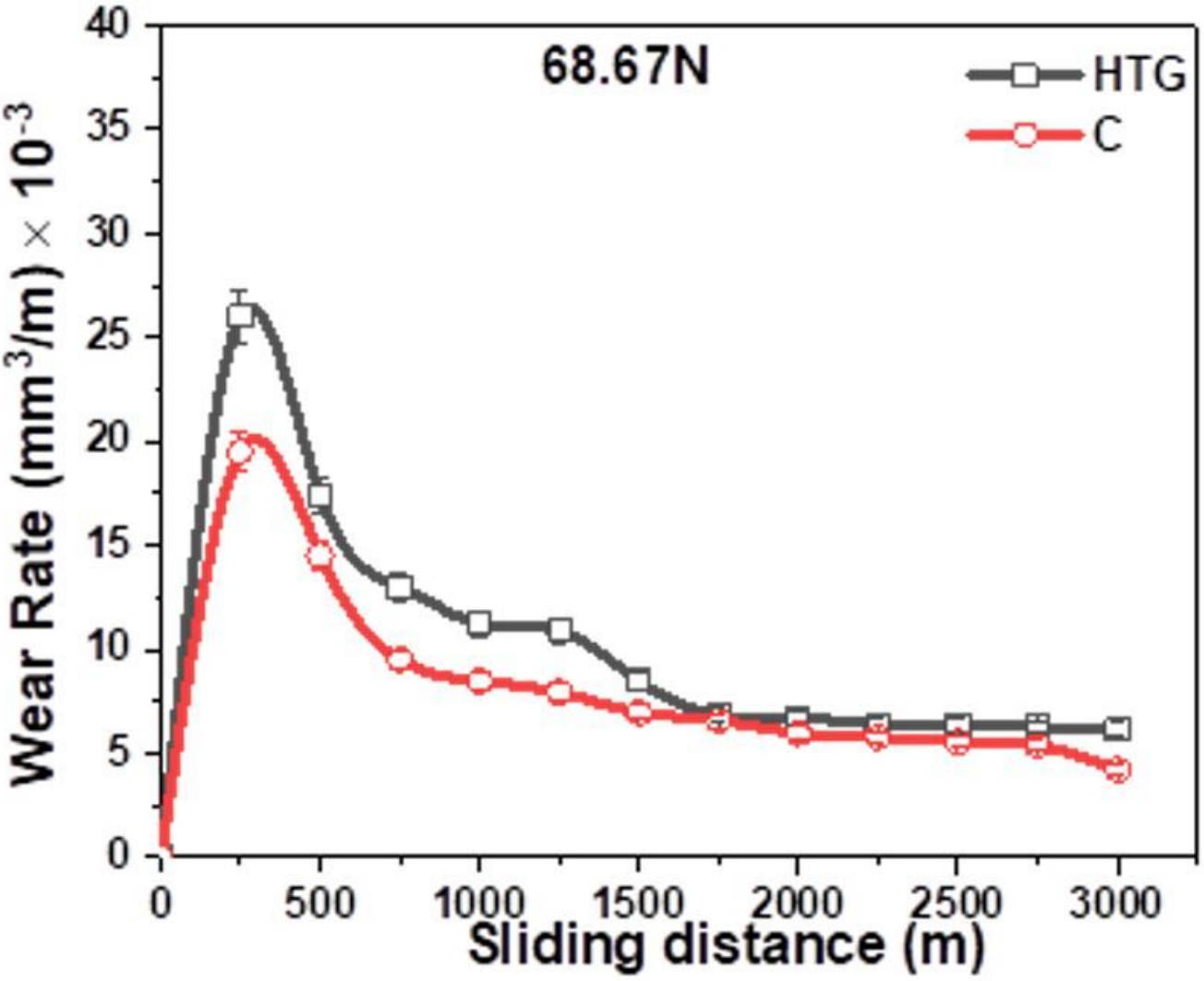

Figure 11

Comparative wear performance of HTG and Cast iron (C).

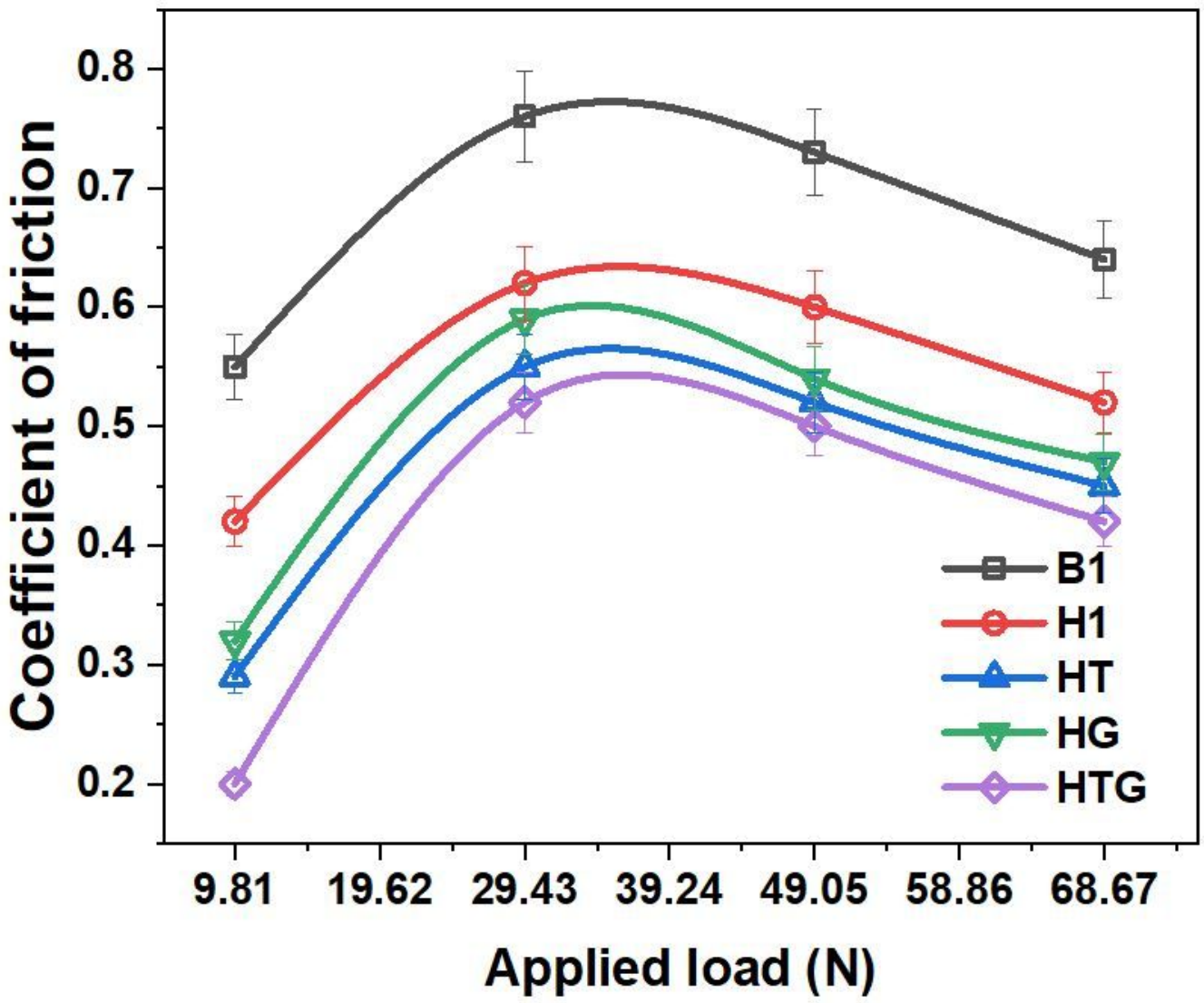

Figure 12

Representing the Coefficient of friction of prepared samples.

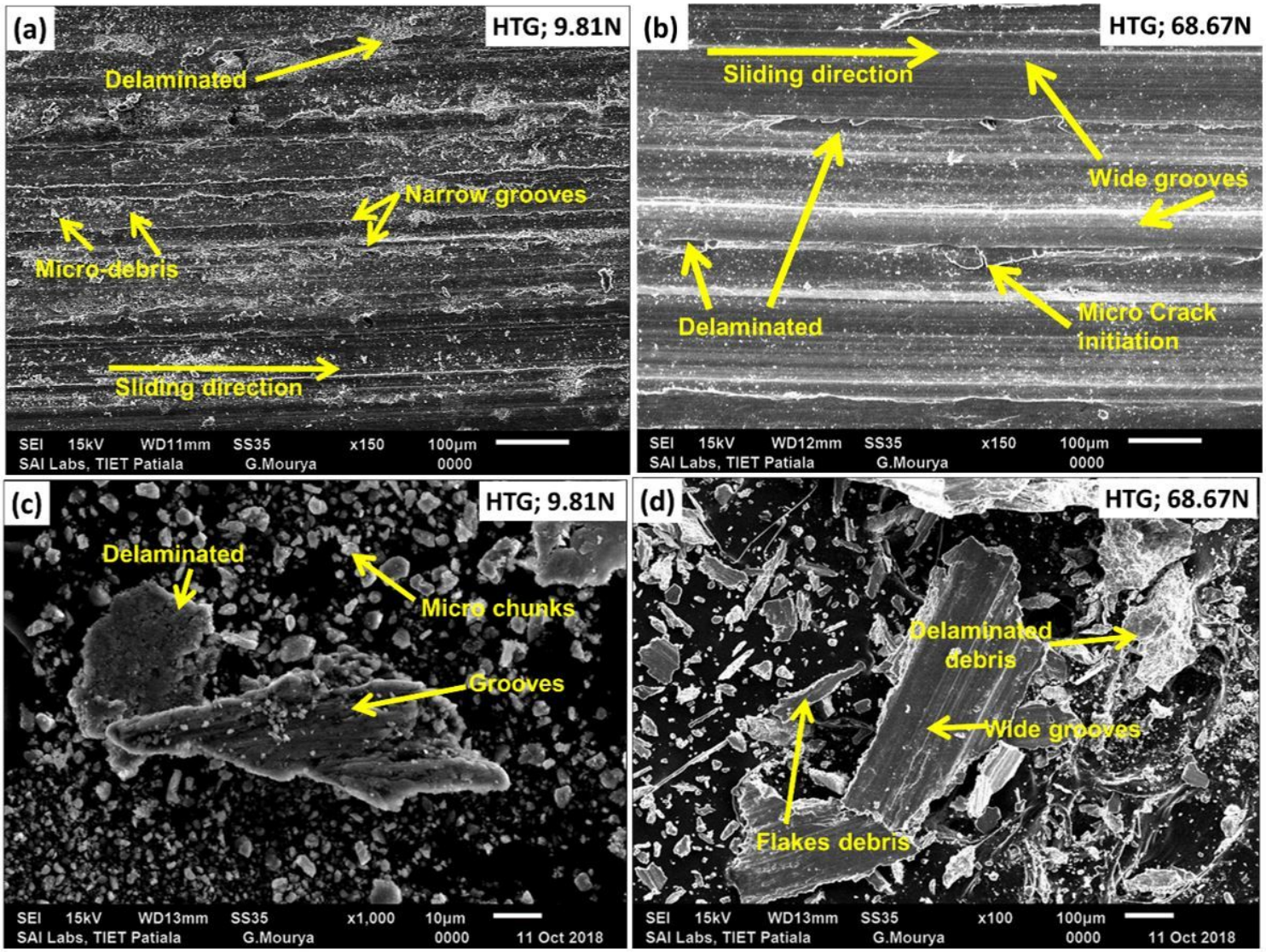

Figure 13

Representing the SEM images of HTG sample (a, b) wear track at 9.81 N and 68.67 N load (c, d) wear debris at 9.81 N and 68.67 N load.

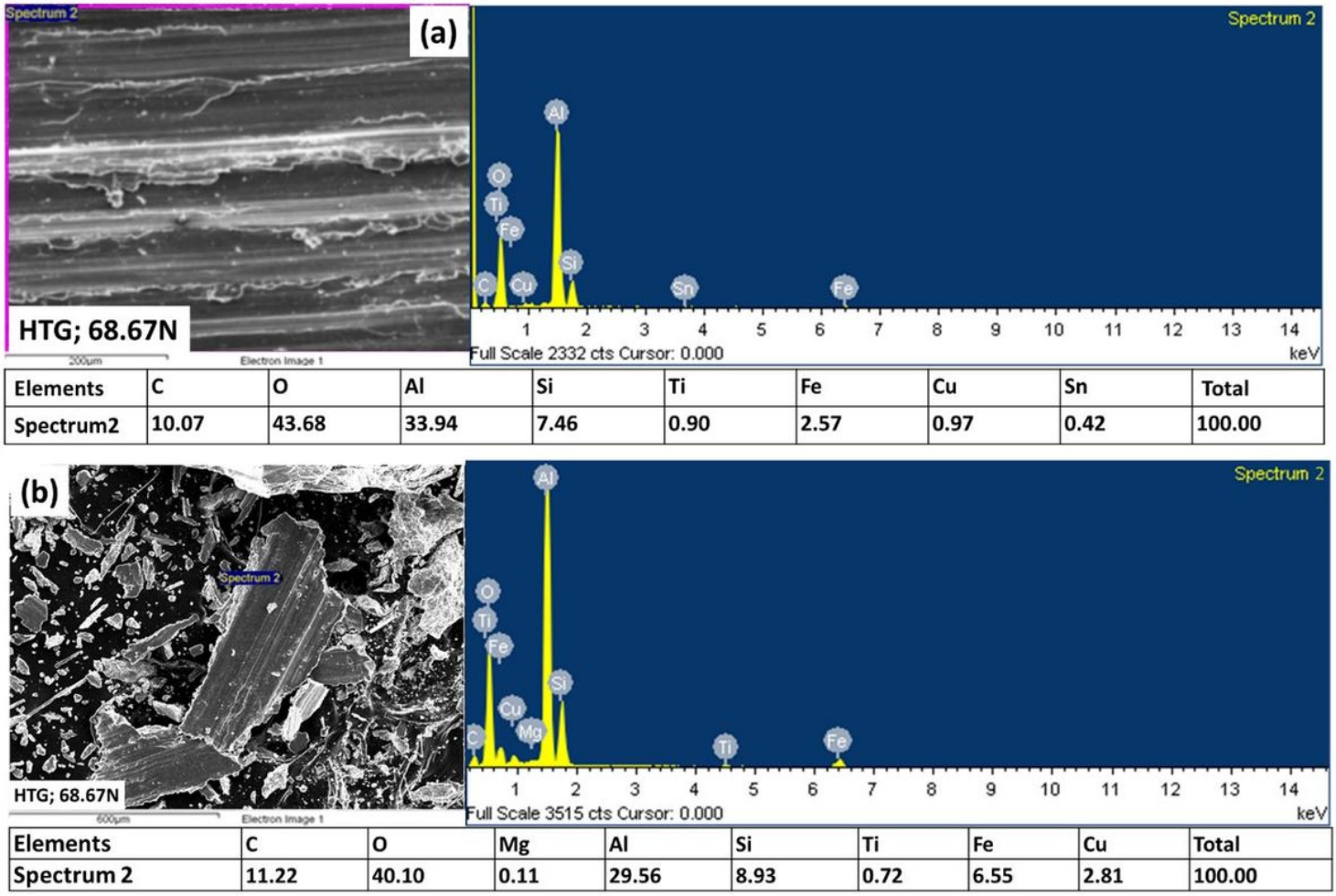

Elements	C	O	Al	Si	Ti	Fe	Cu	Sn	Total
Spectrum2	10.07	43.68	33.94	7.46	0.90	2.57	0.97	0.42	100.00

Elements	C	O	Mg	Al	Si	Ti	Fe	Cu	Total
Spectrum 2	11.22	40.10	0.11	29.56	8.93	0.72	6.55	2.81	100.00

Figure 14

EDS spectrum analysis of HTG sample (a) wear track (b) wear debris at 68.67 loads.